



Eddy-Driven Buoyancy Gradients on Eastern Boundaries and Their Role in the Thermocline

PAOLA CESSI AND CHRISTOPHER L. WOLFE

Scripps Institution of Oceanography, University of California, San Diego, La Jolla, California

(Manuscript received 18 June 2008, in final form 23 January 2009)

ABSTRACT

It is demonstrated that eddy fluxes of buoyancy at the eastern and western boundaries maintain alongshore buoyancy gradients along the coast. Eddy fluxes arise near the eastern and western boundaries because on both coasts buoyancy gradients normal to the boundary are strong. The eddy fluxes are accompanied by mean vertical flows that take place in narrow boundary layers next to the coast where the geostrophic constraint is broken. These ageostrophic cells have a velocity component normal to the coast that balances the geostrophic mean velocity. It is shown that the dynamics in these thin ageostrophic boundary layers can be replaced by *effective boundary conditions* for the interior flow, relating the eddy flux of buoyancy at the seaward edge of the boundary layers to the buoyancy gradient along the coast. These effective boundary conditions are applied to a model of the thermocline linearized around a mean stratification and a state of rest. The linear model parameterizes the eddy fluxes of buoyancy as isopycnal diffusion. The linear model produces horizontal gradients of buoyancy along the eastern coast on a vertical scale that depends on both the vertical diffusivity and the eddy diffusivity. The buoyancy field of the linear model agrees very well with the mean state of an eddy-resolving computation. Because the east–west difference in buoyancy is related to the zonally integrated meridional velocity, the linear model successfully predicts the meridional overturning circulation.

1. Introduction

One measure of the strength of the meridional transport in the ocean is the meridional overturning circulation (MOC), defined here as the time-averaged and zonally integrated meridional mass transport of the ocean.

Monitoring the MOC is observationally challenging; there have been efforts to estimate its transport using a carefully designed set of sustained observations [e.g., the rapid climate change programme (RAPID)]. Using geostrophy of the meridional velocity and mass conservation, it is possible to obtain an approximate estimate of the zonally integrated transport streamfunction by knowing the wind stress forcing and the buoyancy difference across the basin (i.e., the buoyancy on the eastern and western boundaries; Hirschi and Marotzke 2007; Marotzke 1997). Defining the meridional transport streamfunction, Ψ , such that

$$\Psi_z \equiv - \int_{x_w}^{x_e} v \, dx, \quad (1)$$

it is possible to relate Ψ to the wind stress, τ , distributed over the Ekman layer as a body force, and the difference in buoyancy on the eastern and western coasts, $\Delta b \equiv b_e - b_w$. In particular, if the ocean's bottom at $z = -H$ is flat, then

$$f\Psi \approx \left(\frac{z}{H} + 1\right) \int_{-H}^0 d\hat{z} \int_{-H}^{\hat{z}} \Delta b \, dz - \int_{-H}^z d\hat{z} \int_{-H}^{\hat{z}} \Delta b \, d\hat{z} + \int_{x_w}^{x_e} \left[\tau - \left(\frac{z}{H} + 1\right) \tau \Big|_{z=0} \right] dx. \quad (2)$$

The diagnostic (2) needs to be revised in the presence of bottom relief, in which case Ψ is not fully determined by τ and Δb (Hirschi and Marotzke 2007). Comparisons with ocean models indicate that the approximation (2) works very well when the bottom is flat and captures the time variability of the MOC even with topography. In the case where the bottom is flat the diagnostic (2) is very accurate, as illustrated in Fig. 1, which compares Ψ from (1) with the approximation

Corresponding author address: Paola Cessi, 9500 Gilman Drive, UCSD-0213, La Jolla, CA 92093-0213.
E-mail: pcessi@ucsd.edu

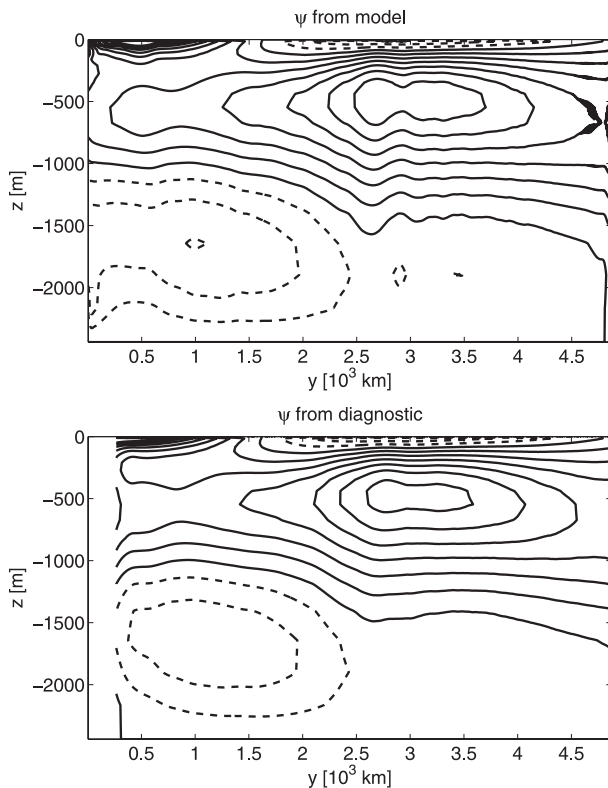


FIG. 1. The overturning streamfunction Ψ for an eddy-resolving computation forced by wind stress and prescribed surface buoyancy. Only the Northern Hemisphere portion of the domain is depicted here. The actual model has two hemispheres of equal extent, with the southernmost 1200 km of the domain occupied by a reentrant channel. The parameters of the model are described in appendix A. (top) The actual transport of the MOC, defined by (1), and (bottom) the diagnostic (2). The diagnostic is an excellent approximation, except at the equator, where f vanishes. The contour interval (CI) is 1 Sverdrup ($\text{Sv} \equiv 1 \times 10^6 \text{ m}^3 \text{ s}^{-1}$) and negative values are dashed.

(2) for an eddy-resolving computation [cf. appendix A and Wolfe and Cessi (2009)].

Theories of the ideal thermocline assume that the buoyancy on the eastern boundary is a function of depth only and does not depend on the latitudinal position along the boundary (Welander 1971; Rhines and Young 1982; Luyten et al. 1983). This unrealistic assumption eliminates the contribution to the MOC from the eastern boundary buoyancy. The assumption arises from the requirement that horizontal flow is in thermal wind balance (i.e., geostrophic and hydrostatic) near the eastern boundary and from the condition of no normal flow into the coast.

The structure of the buoyancy on the eastern boundary is of importance not just for the MOC, but also for the horizontal large-scale circulation of the interior basin. Indeed, below the Ekman layer the flow approximately

conserves potential vorticity (PV), which is qualitatively determined by the planetary term, βy . This implies that potential vorticity contours in contact with the eastern boundary (“blocked contours” in the language of Rhines and Young 1982) carry the information about buoyancy into the interior. As a result, if the buoyancy at the eastern wall is independent of the horizontal position along the boundary, then the interior is at rest as well (the “shadow zone” in the language of Luyten et al. 1983).

The requirement that buoyancy is independent of latitude, y , along the eastern wall clashes with the necessity of allowing buoyancy to depend on y at the surface: how can the isopycnals, independent of latitude on the eastern wall, match the surface values at the intersection of the eastern boundary with the surface? This contradiction is reconciled in classical thermocline theories by allowing “weak solutions,” that is, solutions that have discontinuous buoyancy (or discontinuous derivatives) at the intersection of the surface with the eastern wall. Thus, without vertical diffusion, solutions of the ideal thermocline equations are discontinuous all along the surface marking the boundary between the region of horizontal flow and the quiescent abyss: this is because this boundary has to be a surface of constant density, but it is in general not at a constant depth, while in the quiescent abyss density depends on depth only. The addition of vertical diffusion, with diffusivity κ_v , allows an internal boundary layer of thickness proportional to $\sqrt{\kappa_v}$ to smooth the transition (Stommel and Webster 1962; Young and Ierley 1986; Salmon 1990; Samelson and Vallis 1997). However, the singularity at the boundary between the surface and the eastern coast is not cured by vertical diffusion (cf. Gill 1985, hereafter referred to as G85).

The crowding of isopycnals at the boundary between the surface and the eastern wall, implicit in weak solutions, is a configuration rich in available potential energy (APE). We thus expect the region near the eastern boundary to be baroclinically unstable. Indeed, the analysis of global altimetric data shows secondary maxima of eddy-kinetic energy (EKE) near the eastern boundaries of all oceans, albeit weaker than the maxima on the western boundaries (Stammer 1997). A similar enhancement of EKE near the eastern boundary is found in eddy-resolving simulations of the wind and buoyancy-driven circulation. This is illustrated in Fig. 2, which shows the vertically averaged EKE for an eddy-resolving computation (cf. Wolfe and Cessi 2009). The release of APE is accompanied by a flattening of the isopycnals, leading to horizontal buoyancy gradients on the eastern and western boundaries. Figure 3 shows the time-averaged buoyancy on the

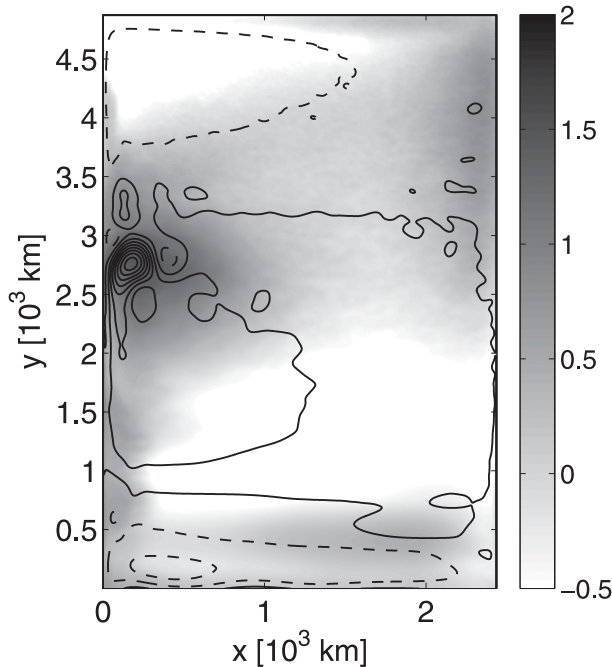


FIG. 2. The vertically averaged EKE is shown in grays (\log_{10} scale) for the Northern Hemisphere part of eddy-resolving computation described in appendix A. The contours of the barotropic streamfunction are shown in black. Notice the EKE maxima on the eastern side of the subpolar gyre and on the western side of the subtropical gyre.

eastern and western boundaries for an eddy-resolving computation. Eddy buoyancy (and momentum) fluxes are associated with the field of mesoscale eddies near the boundaries.

In this work we show that the eddy fluxes of buoyancy drive an ageostrophic circulation with a velocity component into and out of the boundary, which balances the corresponding geostrophic flow. In this way, the condition of no flow into the solid boundary can be fulfilled while maintaining a horizontal buoyancy gradient on the wall. Then an east–west buoyancy difference, Δb , can be supported and we show how Δb can be predicted. This allows the overturning streamfunction, Ψ , to be evaluated from (2).

A theory for Δb is developed, which is a simple extension of the linear thermocline equations used by G85, augmented by eddy fluxes of buoyancy (parameterized as isopycnal buoyancy diffusion) and viscosity.

Numerical solutions of the noninertial thermocline equation naturally include horizontal diffusion, and thus have meridional buoyancy variations on the eastern boundary (Colin de Verdière 1989; Salmon 1990; Samelson and Vallis 1997). In this study we offer an explicit scaling for the depth of penetration of surface buoyancy gradients on the eastern wall and

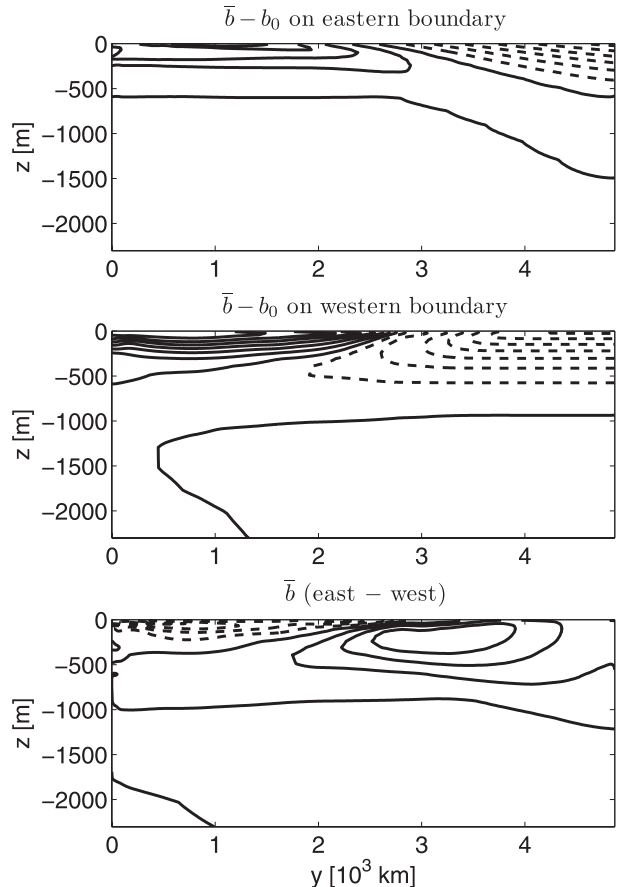


FIG. 3. The time-averaged buoyancy minus the time and horizontally averaged field, $\bar{b}(x, y, z) - b_0(z)$, for an eddy-resolving computation driven by wind stress and surface buoyancy. (top) Here, $\bar{b} - b_0$ on the eastern boundary, $x = x_e$; (middle) $\bar{b} - b_0$ on the western boundary, $x = 0$; (bottom) the difference between the fields in (top) and (middle), i.e., $\bar{b}(x_e, y, z) - \bar{b}(0, y, z)$. The vertical extent of buoyancy gradients is larger on the western boundary compared to the eastern boundary. The difference field shows two overturning cells: a shallow, thermally indirect cell in the subtropics and a deeper, thermally direct cell centered in the subpolar gyre. The CI for all three panels is $2 \times 10^{-3} \text{ m s}^{-2}$. Negative values are dashed.

illustrate how this depth affects the interior buoyancy distribution.

2. Eddy fluxes near the boundaries

The release of APE at the mesoscale and the associated flattening of the buoyancy field is accompanied by eddy fluxes of momentum and buoyancy. The eddy fluxes of momentum break the geostrophic constraint and the eddy buoyancy fluxes induce a time-averaged ageostrophic circulation as shown below.

At the solid boundaries the velocity field must satisfy nonnormal flow (and, less importantly, no-slip boundary), and there must be no flux of buoyancy into the wall.

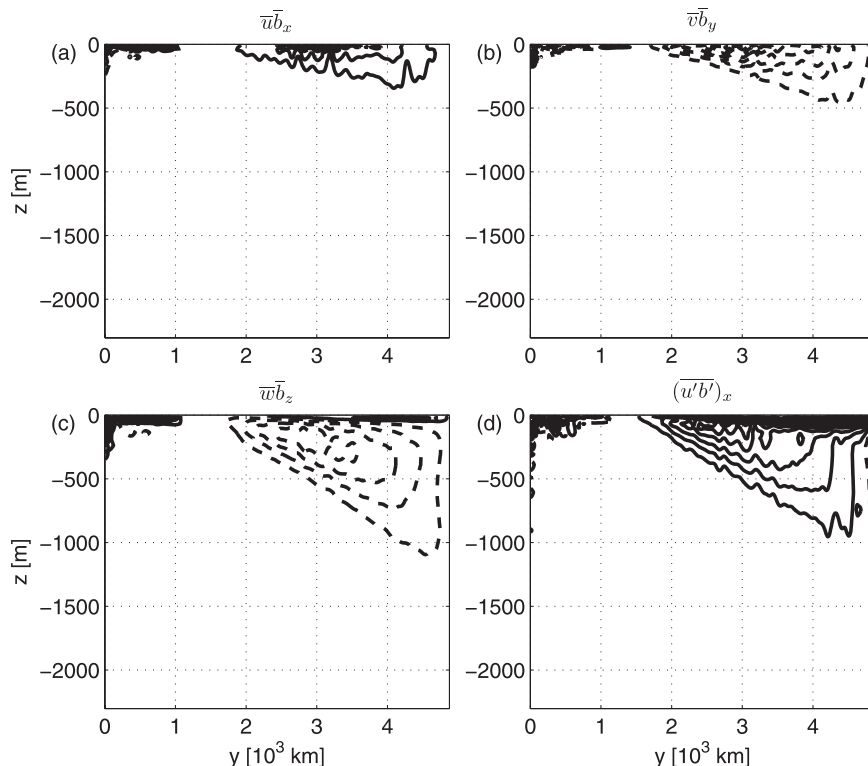


FIG. 4. The mean buoyancy balance near the eastern boundary for the eddy-resolving computation is illustrated by showing the four largest terms 45 km west of the eastern boundary. The main balance is between (bottom) $\overline{(u'b')_x}$ and $\overline{w'b'_z}$. (top) The terms $\overline{u'b'_x}$ and $\overline{v'b'_y}$ are smallest and tend to cancel each other. The terms $\overline{(v'b')_y}$, $\overline{(w')_z}$, and $\kappa_v \overline{b'_{zz}}$ are all smaller than any of the terms shown here. The terms are smoothed with a 20-point Hanning window in the y direction to remove grid noise excited by hydrostatic convection. The parameters of the model are described in appendix A.

In general, these conditions are fulfilled in thin boundary layers where geostrophy is broken. In our numerical simulations we find that in these thin boundary layers, Reynolds stresses become large in the alongshore momentum balance, while the across-shore balance remains geostrophic. In this way, the velocity along the boundary is geostrophic but the component normal to the boundary is not. This is the common expectation on the western boundary, and here we find that semigeostrophy is also the case on the eastern side.

Near the eastern boundary the buoyancy balance is approximately

$$\overline{(u'b')_x} + \overline{w'b'_z} \approx 0, \quad (3)$$

where the overbar denotes a time average and the primes denote the departure from time average. The balance (3) arises from the assumption that in the boundary layer the component of the buoyancy flux divergence normal to the coast is much larger than that along the coast, and balances the vertical component, dominated by mean

downwelling of buoyancy. Consistently, it is assumed that buoyancy does not change appreciably in the boundary layer, and this is why the term $\overline{u'b'_x}$ is neglected. The dominant balance in (3) is illustrated in Fig. 4, which shows the four largest terms in the time-averaged buoyancy equation near the eastern boundary for the eddy-resolving computation described in appendix A. As assumed in (3), both $\overline{u'b'_x}$ and $\overline{v'b'_y}$ are smaller than $\overline{w'b'_z}$. Furthermore, there is a substantial cancellation between $\overline{u'b'_x}$ and $\overline{v'b'_y}$, so that their sum is even smaller than each individual term. This is not surprising: near the eastern boundary the horizontal flow is dominated by the baroclinic component, which is in thermal wind balance, and thus largely orthogonal to the horizontal buoyancy gradient. The diagnostic in Fig. 4 confirms that the eddy-induced overturning circulation in the boundary layer is essentially two-dimensional in the x - z plane.

By continuity, the upwelling, \overline{w} , has to be accompanied by a horizontal mass divergence, which near the boundary is dominated by the component normal to the boundary:

$$\bar{w}_z + \bar{u}_x \approx 0. \tag{4}$$

It might seem surprising that the mean velocity along the boundary is negligible in this region, but in section 3b we formally show that there is a scaling such that the mean buoyancy varies little across the upwelling layer. Thus, the mean alongshore velocity \bar{v} (in geostrophic balance) is not especially large and \bar{v}_y is smaller than \bar{u}_x in the boundary layer (i.e., the circulation is approximately two-dimensional).

Eliminating \bar{w} between (3) and (4) and integrating across the upwelling boundary layer we find that at the seaward edge of the boundary layer

$$\left(\frac{\overline{u'b'}}{\bar{b}_z}\right)_z = \bar{u}. \tag{5}$$

Taking the z derivative of (5) and using thermal wind balance, applicable outside the boundary layer, we find

$$\left(\frac{\overline{u'b'}}{\bar{b}_z}\right)_{zz} = -\frac{\bar{b}_y}{f}. \tag{6}$$

This is the *effective boundary condition* that applies to the baroclinic flow at the outer edge of the thin upwelling layer [i.e., (6) is the boundary condition (BC) felt by the interior flow]. Physically, (6) arises from a balance between the ageostrophic zonal velocity associated with the upwelling necessary to balance the baroclinic fluxes and the geostrophic zonal velocity in thermal wind balance.

An analogous calculation can be repeated at a northern or southern boundary, and in general, assuming that the tangential component of the wind stress vanishes at the coast, the effective boundary condition is

$$\left(\frac{\overline{\mathbf{u}'b'} \cdot \hat{\mathbf{n}}}{\bar{b}_z}\right)_{zz} = -\frac{\nabla \bar{b} \cdot \hat{\mathbf{s}}}{f} \text{ on the boundaries.} \tag{7}$$

In (7), $\hat{\mathbf{n}}$ and $\hat{\mathbf{s}} \equiv \hat{\mathbf{z}} \times \hat{\mathbf{n}}$ are the outward normal and tangent unit vectors on the boundary, respectively. The eddy fluxes of buoyancy maintain an ageostrophic circulation in thin boundary layers near the walls that is equal and opposite to the geostrophic mean flow on the boundary, so that the condition of nonnormal flow can be satisfied while also having a buoyancy gradient along the boundary. Consistent with the intuitive notion of baroclinic instability, a buoyancy gradient along the boundary is necessary if the eddies are to reduce the APE and restratify the buoyancy near the coast, deepening the region where the surface buoyancy distribution penetrates.

The effective boundary condition (5) on b affects the *baroclinic* component of the flow, not the barotropic one. A cancellation between the geostrophic and ageostrophic velocity is only admissible for the baroclinic component of the velocity. This is because the mean ageostrophic horizontal velocity, \bar{u} , in (4) must have zero vertical average. The mean barotropic component of the flow remains geostrophic all the way into the eastern boundary layer and the barotropic streamfunction is constant along the eastern boundary.

The effective boundary condition (7) is not very accurate near the western boundary, where advection of buoyancy and momentum by the mean flow is important. The advection by a barotropic boundary current is easily included in the effective boundary condition, but this effect is not considered here and is deferred to a future study.

3. A linear model of the thermocline

We illustrate the consequences of the effective boundary conditions just derived in a simple buoyancy and wind-driven laminar model, where the eddy flux of buoyancy is parameterized as isopycnal diffusion and the eddy fluxes of momentum are parameterized as downgradient momentum diffusion. To make the calculation amenable to semianalytic progress, we linearize the buoyancy around a prescribed mean stratification, N^2 , as in the G85 model.

G85's model considers the circulation driven by Ekman pumping in the context of noninertial planetary geostrophy, and we add lateral viscosity to fulfill the conditions of nonnormal flow and no-slip ($u = v = 0$ on all solid boundaries). Thus the momentum and mass balances are given by

$$-fv = -p_x + \tau_z + \nu \nabla^2 u, \tag{8}$$

$$fu = -p_y + \nu \nabla^2 v, \tag{9}$$

$$0 = -p_z + b, \tag{10}$$

$$0 = u_x + v_y + w_z. \tag{11}$$

The notation is standard: we use a Cartesian, equatorial β plane, $f = \beta y$, and the east–west wind stress divided by the Boussinesq density, τ , is applied as a body force that decays rapidly from the surface, $z = 0$. These are the same equations used in noninertial thermocline theories (Salmon 1986; Colin de Verdière 1988; Salmon 1990; Samelson and Vallis 1997).

In the linear case, without topography, the barotropic mode can be calculated independently of the baroclinic motion by vertically integrating (8) and (9). Denoting

the barotropic streamfunction with ψ , we have the standard barotropic mode equation

$$\beta\psi_x = -\tau(x, y, 0)_y/H + \nu\nabla^4\psi. \quad (12)$$

Typical solutions of (12) are discussed in Pedlosky (1987). Here we are interested in the buoyancy distribution, and thus the baroclinic flow, which is forced by gradients of the buoyancy, b , in hydrostatic balance.

Assuming that the viscous terms are important only in boundary layers where the alongshore velocity is in planetary-geostrophic balance, the baroclinic system (8)–(11) can be manipulated to eliminate u and v in favor of b and w to give the vorticity equation. The full derivation is given in appendix B.

For the purpose of this study, we consider an approximate form of the vorticity equation that allows application of the nonnormal flow condition, but not of the no-slip condition:

$$\beta\frac{b_x}{f^2} = w_{zz} - \left(\frac{\tau_{zz}}{f}\right)_y + \nu\nabla \cdot \left[\frac{1}{f}\nabla^2\left(\frac{\nabla b}{f}\right)\right] + O(\nu^2). \quad (13)$$

The system is completed by the buoyancy equation, linearized around a state of rest and a mean density b_0 that depends on z only. With $N^2 \equiv db_0/dz$, the perturbation density b is governed by

$$wN^2 = \kappa\nabla^2 b + \kappa_\nu b_{zz}. \quad (14)$$

The neglect of advection of b differentiates this model from most noninertial theories (Colin de Verdière 1988; Salmon 1990; Samelson and Vallis 1997), but it allows analytic progress that is not possible in the nonlinear case.

The second term on the RHS is vertical diffusion of buoyancy. The first term on the RHS of (14) is the parameterization of eddy fluxes of buoyancy. The eddy diffusivity, κ , is taken to be constant (Gent and McWilliams 1990). Because the buoyancy is linearized around $b_0(z)$, isopycnal eddy fluxes are approximately horizontal. If $\mathbf{u}'b' = -\kappa\nabla b$, eddy fluxes are along isopycnals as long as

$$\overline{w'b'} = \kappa|\nabla b|^2/(N^2 + b_z) \approx \kappa|\nabla b|^2/N^2, \quad (15)$$

where the last approximation is made because $b \ll b_0$. If we now compare the horizontal divergence of the horizontal eddy flux with the vertical derivative of the vertical component we find

$$\frac{(\overline{w'b'})_z}{\nabla \cdot (\overline{\mathbf{u}'b'})} \sim \frac{b}{b_0} \ll 1, \quad (16)$$

which is much less than unity in the linearized system. Thus the nonlinear vertical eddy fluxes (15) are neglected in the linear model.

We can use (14) to eliminate w in favor of b in (13) to obtain

$$\beta\frac{b_x}{f^2} = \left(\frac{\kappa\nabla^2 b + \kappa_\nu b_{zz}}{N^2}\right) - \left(\frac{\tau_{zz}}{f}\right)_y + \nu\nabla \cdot \left[\frac{1}{f}\nabla^2\left(\frac{\nabla b}{f}\right)\right]. \quad (17)$$

The system (8)–(11) and (14) has been studied before as a model of the thermocline. Pedlosky (1969) provided a preliminary analysis of the interior solution and the structure of the boundary layers. Pedlosky's parameter ordering was such that buoyancy gradients on the eastern boundary were excluded. Salmon (1986) has studied the same problem with simplified friction (Rayleigh drag instead of Newtonian friction but non-hydrostatic pressure). Again Salmon assumes that κ is so small that buoyancy gradients on the eastern coast are excluded. More recently, numerical solutions have been obtained with horizontal advection of buoyancy added to (14) (Colin de Verdière 1989; Salmon 1990; Samelson and Vallis 1997), a case not amenable to simple analysis. Our study differs from previous quasi-ideal thermocline solutions in that we stress the role of eddy fluxes of buoyancy near the boundaries (east and west), and thus include horizontal diffusion of buoyancy as a first-order effect. In particular, we emphasize that eddy fluxes are crucial in allowing gradients of buoyancy along the boundaries.

a. The boundary conditions

The system (13) and (14), or alternatively (17), needs two boundary conditions on each of the two boundaries $z = 0$ and $z = -H$, and two horizontal BC on each of the four boundaries $x = 0, x_e$ and $y = 0, L$. The vertical BC are the specification of b and the requirement that $w = 0$, that is,

$$b = g'B(y) \quad \text{at } z = 0; \quad b = 0 \quad \text{at } z = -H, \quad (18)$$

$$\begin{aligned} \kappa\nabla^2 b + \kappa_\nu b_{zz} &= 0 \quad \text{at } z = 0; \\ b_{zz} &= 0 \quad \text{at } z = -H. \end{aligned} \quad (19)$$

The function B gives the nondimensional form of the surface buoyancy, whose magnitude is given by g' . The lateral BC are $\mathbf{u} \cdot \hat{\mathbf{n}} = 0$ and $\nabla b \cdot \hat{\mathbf{n}} = 0$ on $x = 0, x_e$ and $y = 0, L$. The nonnormal flow condition can be stated in terms of b using (9):

$$\nabla b \cdot \hat{\mathbf{s}} = \tau_{zz} \cdot \hat{\mathbf{s}} + \nu \left[\nabla^2 \left(\frac{\nabla b}{f} \right) \cdot \hat{\mathbf{n}} \right] \quad \text{on the boundaries.} \quad (20)$$

The outward normal direction is $\hat{\mathbf{n}}$ and the horizontal tangent direction on the boundary is $\hat{\mathbf{s}} \equiv \hat{\mathbf{z}} \times \hat{\mathbf{n}}$. Here we have included the contribution of an alongshore wind stress $\boldsymbol{\tau} \cdot \hat{\mathbf{s}}$.

b. Canonical scaling and effective boundary conditions

The formulation (17) with BC in (19) and (20) has been considered before (Pedlosky 1969; LaCasce 2004). These authors have considered the regime where $\nu \approx \kappa$, so that the horizontal diffusion is only important in viscous boundary layers and the interior satisfies the balance studied by G85:

$$\beta b_x = f^2 \kappa_\nu (b_{zz}/N^2)_{zz}. \quad (21)$$

The same ordering, or even $\kappa \ll \nu$, has been considered in a numerical solution of the noninertial thermocline equation (Colin de Verdière 1989; Salmon 1990; Samelson and Vallis 1997). Here instead, we consider $\nu \ll \kappa$, so that eddy diffusion, κ , is important in the interior, while the influence of viscosity, ν , is confined to thin side boundary layers. In this case, it is possible to eliminate the viscosity from the description of the interior flow by integrating over the viscous boundary layers and to apply effective boundary conditions on the interior flow that are independent of ν . To do that we begin by scaling (17), so that there are only two parameters in the problem. We will also assume that the stratification, N^2 , is constant.

We use the following nondimensionalization:

$$b = g' \hat{b}, \quad x = l \hat{x}, \quad y = L \hat{y}, \quad z = h \hat{z} \quad (22)$$

where l and h are

$$l \equiv \left(\frac{\beta L^2 \kappa^2}{N^2 \kappa_\nu} \right)^{1/3}, \quad h \equiv \left(\frac{\beta L^2 \sqrt{\kappa \kappa_\nu}}{N^2} \right)^{1/3}. \quad (23)$$

The vorticity equation becomes

$$\frac{\hat{b}_x}{\hat{y}^2} = (\hat{\nabla}^2 \hat{b} + \hat{b}_{zz})_{zz} - \mu \left(\frac{\hat{\tau}_{zz}}{\hat{y}} \right)_{\hat{y}} + \epsilon^2 \hat{\nabla} \cdot \left[\frac{1}{\hat{y}} \hat{\nabla}^2 \left(\frac{\hat{\nabla} b}{\hat{y}} \right) \right]. \quad (24)$$

With the scaling (23), the advection of planetary vorticity, the contribution to vortex stretching by eddy diffusion, and diapycnal mixing all appear without any parameter. There are two external parameters: μ measures the importance of wind stress (of magnitude τ_0) and ϵ measures the importance of viscosity ν . Their definitions are

$$\mu \equiv \frac{\tau_0 l}{g' h^2}, \quad \epsilon^2 \equiv \frac{\nu}{\beta l^3}. \quad (25)$$

In addition, the nondimensional Laplacian contains the aspect ratio of the zonal scale, l , to the scale of the buoyancy forcing, L ; that is,

$$\hat{\nabla} \equiv \partial_{\hat{x}}^2 + \frac{l^2}{L^2} \partial_{\hat{y}}^2. \quad (26)$$

Using values of the parameters as in the eddy-resolving model described in appendix A, we find

$$h \sim 360 \text{ m}, \quad l \sim 1300 \text{ km}, \quad \mu \sim 0.06, \quad \epsilon^2 \sim 2.6 \times 10^{-7}. \quad (27)$$

Notice that the canonical width l is much larger than a boundary layer, although not quite as large as the basin scale, x_e . Similarly, the vertical scale, h , is more than a thin mixed layer, although much less than the depth of the domain. Finally, the parameter measuring the wind forcing versus the buoyancy forcing is substantially less than unity, indicating that over the scales l and h the mechanical forcing is subdominant.

In anticipation of the smallness of the aspect ratio l/L , we focus on the east and west BC (20), whose nondimensional form is

$$\hat{b}_{\hat{y}} = \epsilon^2 \left[\hat{\nabla}^2 \left(\frac{\hat{b}_x}{\hat{y}} \right) \right] \quad \text{and} \quad \hat{b}_{\hat{x}} = 0 \quad \text{at} \quad \hat{x} = 0, X_e, \quad (28)$$

where $X_e \equiv x_e/l$ is another parameter in the problem. On the top and bottom we have

$$\hat{b} = B(\hat{y}) \quad \text{at} \quad \hat{z} = 0; \quad \hat{b} = 0 \quad \text{at} \quad \hat{z} = -\hat{H}, \quad (29)$$

$$\hat{\nabla}^2 B + \hat{b}_{zz} = 0 \quad \text{at} \quad \hat{z} = 0; \quad \hat{b}_{zz} = 0 \quad \text{at} \quad \hat{z} = -\hat{H}, \quad (30)$$

where the notation $\hat{H} \equiv H/h$ has been adopted.

The BC of no flux of buoyancy and nonnormal flow (28) are both conditions on the derivatives of buoyancy normal to the boundary, so in the viscous boundary layer, only the *normal derivatives* of \hat{b} are changed at $O(1)$, but the value of \hat{b} is only slightly altered. Specifically, in the viscous boundary layer the balance in the vorticity Eq. (24) is between viscosity and lateral diffusion (Barcilon and Pedlosky 1967; LaCasce 2004; Pedlosky and Spall 2005), that is, $\hat{b}_{xxzz} \approx -\epsilon^2 \hat{b}_{xxxx}/\hat{y}^2$. Thus the boundary layer width is given by ϵ . Because the boundary layer correction accommodates the gradients of b , without changing the value of b to leading order in ϵ , the buoyancy can be rewritten as

$$\hat{b} = b_I(\hat{x}, \hat{y}, \hat{z}) + \epsilon \tilde{b}(\xi, \hat{y}, \hat{z}), \quad (31)$$

where b_I is the buoyancy in the interior, $\xi \equiv x/\epsilon$ is the boundary layer variable, and $\epsilon \tilde{b}$ is the boundary layer correction, small in order to correct the derivative, $\hat{b}_{I\xi}$, to

leading order but not the function, b_l . With this scaling (24) becomes

$$\hat{b}_{\xi\xi z z} + \hat{b}_{\xi\xi\xi\xi}/\hat{y}^2 = 0 + O(\epsilon), \quad (32)$$

and the BC (28) becomes

$$b_{I\hat{y}} = \tilde{b}_{\xi\xi\xi\xi}/\hat{y} \quad \text{and} \quad b_{I\hat{x}} + \tilde{b}_{\xi} = 0 \quad \text{at} \quad \hat{x} = 0, X_e. \quad (33)$$

We can now integrate (32) across the boundary layer¹ to find, to leading order in ϵ ,

$$0 = (b_{I\hat{x}} + \tilde{b}_{\xi})_{z z} \Big|_{\xi=" \infty"}^{x=0} + \frac{\tilde{b}_{\xi\xi\xi\xi}}{\hat{y}^2} \Big|_{\xi=" \infty"}^{x=0} + O(\epsilon), \quad (34)$$

where $\xi = " \infty"$ is the seaward edge of the boundary layer. Using (33) together with the condition that \tilde{b} vanishes as $\xi \rightarrow \infty$, we obtain the effective boundary conditions

$$\hat{y} b_{I\hat{x} z z} = b_{I\hat{y}} \quad \text{at} \quad \hat{x} = 0, X_e. \quad (35)$$

These BC apply to the *inviscid* vorticity equation, that is, to (24) with $\epsilon = 0$, *outside* the viscous boundary layer (i.e., at $\xi = " \infty"$, which is equivalent to $x = 0$, as far as the interior solution is concerned).

In dimensional form, and generalized to all four solid boundaries, the effective boundary conditions are

$$f \left(\frac{\kappa \nabla b \cdot \hat{\mathbf{n}}}{N^2} \right)_{z z} = (\nabla b - \tau_{z z}) \cdot \hat{\mathbf{s}} \quad \text{on the boundaries.} \quad (36)$$

This is just the same as (7), with the eddy flux of buoyancy parameterized as horizontal diffusion. We have also allowed a tangential (alongshore) component of the wind stress at the coast, although this term will be zero in all our subsequent calculations. This term is important in the dynamics of the eastern boundary and will be the subject of a future study.

In the limit of vanishing (or very small) eddy diffusivity, κ , we recover the usual condition that the horizontal derivative of b along the boundary vanishes. This is the laminar thermocline limit that has been examined by several authors (Pedlosky 1969; G85; Salmon 1986; LaCasce 2004; Pedlosky and Spall 2005). All of these previous studies apply the boundary condition $(\nabla b - \tau_{z z}) \cdot \hat{\mathbf{s}} = 0$ on the eastern boundary. The laminar thermocline limit is recovered by considering κ small enough that the canonical l and h are thin boundary layers of no consequence to the interior flow.

¹ Here we integrate across the boundary layer at $x = 0$, but the same procedure is applied on all the boundaries. Advection by the barotropic flow introduces δ_M (and possibly a nonlinear western boundary scale) in the eddy-resolving model.

In the following we show that consideration of eddy processes in the interior of the domain leads to solutions that are qualitatively different than those with no eddy processes.

We thus proceed to solve the interior vorticity equation, which in dimensional form is

$$\beta \frac{b_x}{f^2} = \left(\frac{\kappa \nabla^2 b + \kappa_v b_{z z}}{N^2} \right)_{z z} - \left(\frac{\tau_{z z}}{f} \right)_y, \quad (37)$$

with the effective lateral boundary conditions (36).

c. Relation to G85 scaling

The canonical scales l and h in (23) are a special case of the similarity scaling of G85, given by

$$l^{1/4}/h = r, \quad \text{where} \quad r \equiv \left(\frac{N^2}{\kappa_v \beta L^2} \right)^{1/4}. \quad (38)$$

Notice that the parameter r is independent of κ . G85 looks for similarity solutions satisfying (21) and with the origin of coordinates on the eastern boundary. In other words, G85 looks for solutions of the form

$$b(\eta), \quad \text{where} \quad \eta \equiv -r z (x_e - x)^{-1/4}, \quad (39)$$

and his solutions $b(\eta)$ are singular at $x = x_e$.

We can think of l as the distance over which we need to shift the coordinate x eastward in order to move the singularity outside of the domain (cf. Fig. 5). Then h is the depth of the thermocline at $x = x_e$. Eddy diffusion cures the singularity in G85's solution by allowing a finite depth of the thermocline at $x = x_e$. However, it is not possible to find solutions of (37) in similarity form when horizontal diffusion is included.

For large basins, l is significantly less than the full domain's width, x_e . Therefore for $x_e - x \gg l$, G85's balance (21) applies: as the western boundary, $x = 0$, is approached, the depth of the thermocline is of order h_G , where

$$h_G \equiv \left(\frac{\kappa_v \beta L^2 x_e}{N^2} \right)^{1/4} \quad (40)$$

is G85's depth. This is also the depth of the thermocline found by Pedlosky (1969; l_T in his notation). Clearly, h_G is larger than h , because x_e is larger than l (cf. Fig. 5).

Near the western boundary, eddy effects become important again and we need to satisfy the effective boundary condition (36). Because the depth scale of the incoming flow is $h_G \gg h$, the second term on the RHS of (37) is negligible. Thus the horizontal scale

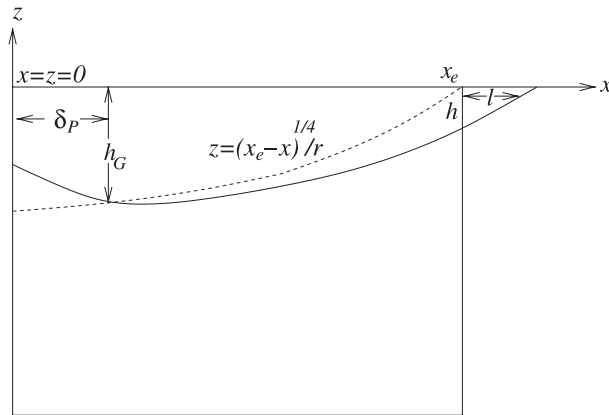


FIG. 5. A sketch of the vertical and horizontal scales of the thermocline. The solid line shows the depth of the thermocline obtained including eddy fluxes of buoyancy. The edge of the thermocline is drawn beyond the eastern boundary to show the relation with the similarity solution of G85, shown as a dashed line. At the eastern boundary, and on a horizontal scale of order l , the depth of the thermocline is order h [cf. (23)]. Within a distance of $O(l)$ of x_e , all three terms in the vorticity Eq. (23) are important. A horizontal distance of order x_e into the domain, the vertical scale is h_G , defined in (40); in this region the eddyless balance examined by G85 is recovered. Within a distance δ_P of the western boundary, eddy fluxes of buoyancy are important again: here the depth of the thermocline is $h_G \gg h$ so diapycnal diffusion is negligible.

near the western boundary is not l , but a new scale δ_P defined as

$$\delta_P \equiv \kappa \left(\frac{\beta L^2}{\kappa_v x_e N^2} \right)^{1/2}. \tag{41}$$

This is one of the possible western boundary layer widths for the baroclinic component of the flow considered by Pedlosky (1969); the other possible width is the Munk scale, $\delta_M \equiv (\nu/\beta)^{1/3}$, but here we consider a parameter ordering such that $\delta_M \ll \delta_P$.

The horizontal scale δ_P is shorter than the eastern boundary scale, because $\delta_P = l h^2/h_G^2$. It is easy to verify that with the horizontal scale δ_P and the vertical scale h_G the alongshore buoyancy gradient is of the same order as the eddy flux term in (36): near the western boundary b changes to leading order over a distance δ_P .

The different scales are illustrated in Fig. 5, which also shows G85’s similarity variable as a dashed line.

In summary, eddy fluxes of buoyancy introduce a new horizontal scale on the eastern boundary, l , associated with the depth of the thermocline, h , at $x = x_e$. On the domain scale, and thus as the western boundary is approached from the east, the thermocline is of depth h_G and eddy fluxes are unimportant in the interior. Within a horizontal distance of order δ_P from the western boundary, eddy fluxes become important again; δ_P is the

western boundary layer width for the buoyancy, and thus for the baroclinic component of the flow—very different from the western boundary layer width of the barotropic flow, δ_M , governed by (12).

d. Method of solution

Here we delineate the method of solutions of the interior vorticity equation, (37), subject to the effective boundary conditions (35). We consider the solutions in nondimensional units, but drop the hats from our notation in this subsection. To allow analytic progress, we consider the limit where the dynamical aspect ratio l/L is much less than one, which is a mild restriction. In this limit, $\nabla^2 \approx \partial_x^2$ and the interior buoyancy satisfies

$$\frac{b_x}{y^2} = (b_{xx} + b_{zz})_{zz} - \mu \left(\frac{\hat{\tau}_{zz}}{y} \right)_y, \tag{42}$$

subject to the BC (30) (with $\nabla^2 \approx \partial_x^2$) and (35).

Assuming that the wind stress acts as a body force confined to a thin Ekman layer of nondimensional depth d with the form $\hat{\tau} = \sigma(y)e^{z/d}$, the solution to (42) can be written as

$$b = b_p(y, z) + \sum_{n=0}^{\infty} [a_n(y)e^{\lambda_e(x-x_e)} + c_n(y)e^{-\lambda_w x}] \text{sink}_n z, \tag{43}$$

where the particular solution b_p is given by

$$b_p = B(y) \left(1 + \frac{z}{\hat{H}} \right) + \mu \left(\frac{\sigma}{y} \right)_y \left[d^2 \left(e^{z/d} - 1 - \frac{z}{\hat{H}} \right) - \frac{z^2}{2} - \frac{z^3}{6\hat{H}} - \frac{\hat{H}}{3} z \right]. \tag{44}$$

The vertical wavenumber $k_n = n\pi/\hat{H}$ is quantized by the depth of the domain, and the homogeneous solution decays from the eastern and western boundaries at the rates

$$\lambda_e(y, n) \equiv \frac{1}{2} \frac{1}{(k_n y)^2} \left(-1 + \sqrt{1 + k_n^6 y^4} \right),$$

$$\lambda_w(y, n) \equiv \frac{1}{2} \frac{1}{(k_n y)^2} \left(1 + \sqrt{1 + k_n^6 y^4} \right). \tag{45}$$

Notice that all λ_e and λ_w are positive for all values of n and y . Also, λ_e is smaller than λ_w for every n and y , so the decay scale on the east, l , is longer than the decay scale on the west, δ_P , as anticipated in section 3c.

The coefficients $a_n(y)$ and $c_n(y)$ are determined by the effective boundary conditions on the eastern and western boundaries, that is,

$$\sum_{n=0}^{\infty} [yk_n^2(\lambda_e a_n - \lambda_w c_n e^{-\lambda_w X_e}) + a_{ny} + (c_n e^{-\lambda_w X_e})_y] \sin k_n z = -b_{py} \quad \text{on } x = X_e, \quad (46)$$

$$\sum_{n=0}^{\infty} [yk_n^2(\lambda_e a_n e^{-\lambda_e X_e} - \lambda_w c_n) + c_{ny} + (a_n e^{-\lambda_e X_e})_y] \sin k_n z = -b_{py} \quad \text{on } x = 0. \quad (47)$$

The system (46) and (47) is a series of coupled first-order ordinary differential equations (ODEs) in y that can be solved by projecting the RHS onto sine modes, that is,

$$yk_n^2(\lambda_e a_n - \lambda_w c_n e^{-\lambda_w X_e}) + a_{ny} + (c_n e^{-\lambda_w X_e})_y = -\frac{2}{\hat{H}} \int_{-\hat{H}}^0 b_{py} \sin k_n z \, dz, \quad (48)$$

$$yk_n^2(\lambda_e a_n e^{-\lambda_e X_e} - \lambda_w c_n) + c_{ny} + (a_n e^{-\lambda_e X_e})_y = -\frac{2}{\hat{H}} \int_{-\hat{H}}^0 b_{py} \sin k_n z \, dz. \quad (49)$$

The integrals in (48) and (49) are calculated analytically with the help of Mathematica's Online Integrator. The ODEs in (48) and (49) must be supplemented by the condition that the buoyancy is continuous all along the boundary of the domain. This requirement guarantees that the area-integrated vertical velocity vanishes at every level.

If eddy diffusion in the meridional direction is negligible near the northern and southern walls, then b does not vary along these boundaries and the continuity requirement amounts to

$$a_n(1 - e^{-\lambda_e X_e}) = c_n(1 - e^{-\lambda_w X_e}) \quad \text{at } y = 0, \quad 1; \quad (50)$$

that is, there is no meridional velocity across the northern or southern boundary at any level.

The ODEs in (48) and (49) are integrated numerically using Matlab's boundary value problem solver `bvp4c`.

4. Results

a. Estimating the parameters N and κ

The solution (43) depends on the ratios $\hat{H} = H/h$ and $X_e = x_e/l$, that is, the ratios of the canonical depth and width to the size of the domain. To determine the linear solution, the values of the basic stratification, N , and of the eddy diffusivity, κ , must be provided. These two parameters are part of the solution in the eddy-resolving model and are obviously not constants.

The horizontally and time-averaged vertical buoyancy gradient for one simulation is shown in Fig. 6. At

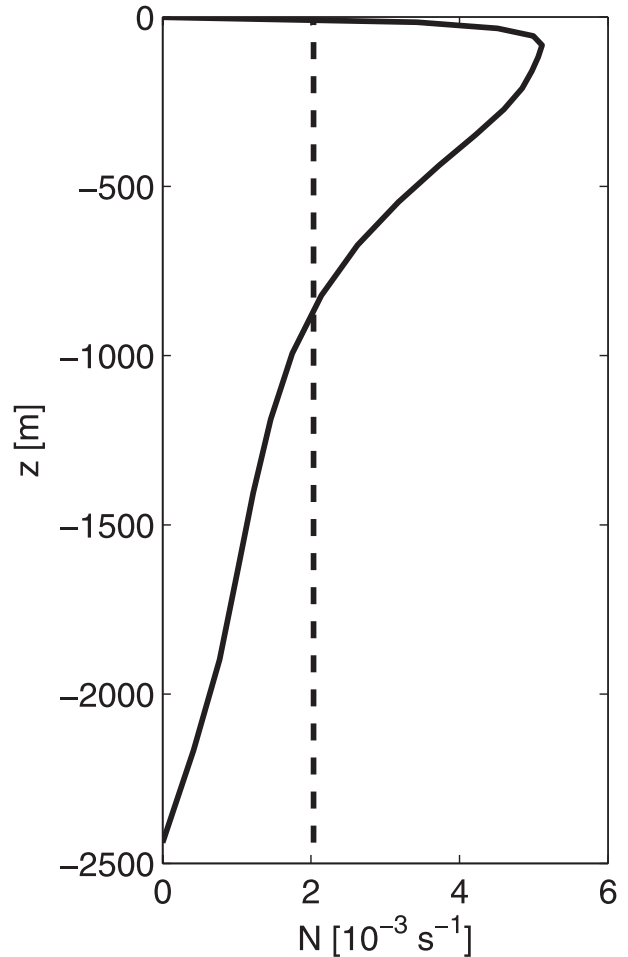


FIG. 6. The mean stratification N of the eddy-resolving model run, defined as the square root of the vertical derivative of the horizontally and time-averaged buoyancy, $N^2 = \langle d\bar{b}/dz \rangle$. The dashed line indicates the vertical average of N . The parameters of the model are described in appendix A.

about 70 m, N has a maximum of about $6 \times 10^{-3} \text{ s}^{-1}$ and then decays with depth to about $2 \times 10^{-3} \text{ s}^{-1}$ at 800 m. The vertically averaged value of N is also indicated in the figure (dashed line), and this is the value that is used to estimate the constant stratification in the linear model (17).

Figure 7 shows a scatterplot of $\overline{u'b'}$ versus \bar{b}_x for two strips near the eastern (top panel) and western (bottom panel) boundaries, each about 250 km wide. The scatter is large and the values differ substantially on the two sides. It is noteworthy that the eddy buoyancy fluxes are higher on the east, although the levels of EKE are higher on the west (cf. Fig. 2). This partition suggests that most of the EKE near the west is generated by barotropic shear instability rather than by baroclinic processes.

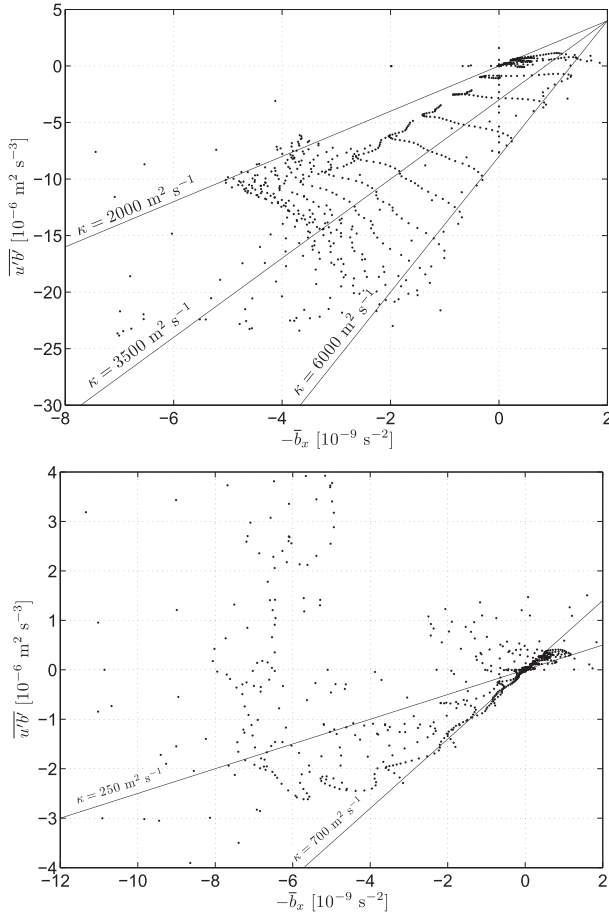


FIG. 7. Scatterplot of $\overline{u'b'}$ vs the time-averaged gradient $\overline{b_x}$ for the eddy-resolving model (dots). The linear slopes (lines) bound most of the points, indicating the range of constant eddy diffusivities found in the computations. (top) Points near the eastern boundary and (bottom) points near the western boundary (within 250 km from the boundaries). Lower slopes are found farther away from the walls. The parameters of the model are described in appendix A.

Because $\overline{u'b'}$ decays away from the boundaries, it is difficult to assign a meaningful constant value for κ : The flux gradient slopes become smaller farther from the boundaries. We use a value of $1200 \text{ m}^2 \text{ s}^{-1}$ as the constant value appropriate for the region of $O(l)$ near the eastern boundary. This value is consistent with the cross-shore diffusivity in the California Current System estimated by Marchesiello et al. (2003) with a high-resolution regional model.

b. A typical solution

In this subsection we present the solutions of the linear model of section 3. As well as the specification of N and κ , the surface buoyancy and the wind stress forcing must be prescribed. We use shapes that are

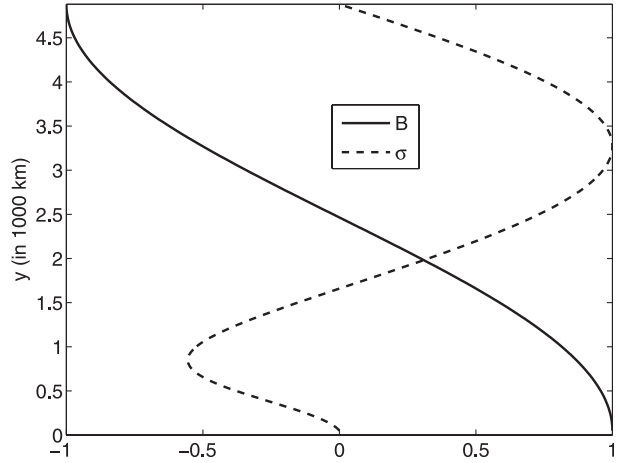


FIG. 8. The shapes of the surface buoyancy B and of the wind stress σ as a function of y ; B satisfies the no-flux condition on the boundaries and σ vanishes on the boundaries.

slight modifications of those used in the eddy-resolving computations² (cf. Fig. 8):

$$b(x, y, 0) = g'B(y) = g' \cos \frac{\pi y}{L},$$

$$\tau = \tau_0 \sigma(y) \hat{e}_d^z = \tau_0 \left[-\cos \frac{3\pi}{2L} y + e^{-\frac{y^2}{2\sigma^2}} \right] \hat{e}_d^z. \quad (51)$$

There is no wind stress at the northern and southern boundaries, to avoid strong upwelling layers, and the surface buoyancy naturally satisfies no flux at the coast.

Figure 9 shows the buoyancy on the eastern and western boundaries for a solution using the same parameter values of the eddy-resolving computation, with N and κ estimated as in section 4a. Other values of the parameters are

$$\kappa_v = 9.8 \times 10^{-5} \text{ m}^2 \text{ s}^{-1}, \quad \beta = 2.3 \times 10^{-11} \text{ s}^{-1} \text{ m}^{-1},$$

$$L = 4.9 \times 10^6 \text{ m}, \quad (52)$$

$$x_e = 2.4 \times 10^6 \text{ m}, \quad g' = 0.016 \text{ m s}^{-2},$$

$$\tau_0 = 1 \times 10^{-4} \text{ m}^2 \text{ s}^{-2}. \quad (53)$$

It is reassuring that the buoyancy signal decays with depth on the scale $h \ll H$, so that the use of a zero buoyancy condition on the bottom is equivalent to the no-flux condition used in the eddy-resolving computation.

A comparison of b_e , b_w , and Δb between the eddy-resolving computation (Fig. 3) and the linear solution

² In the eddy-resolving model the wind stress does not vanish at the equator, but in the linear model it does, so as to ensure some regularity of the solution at the equator.

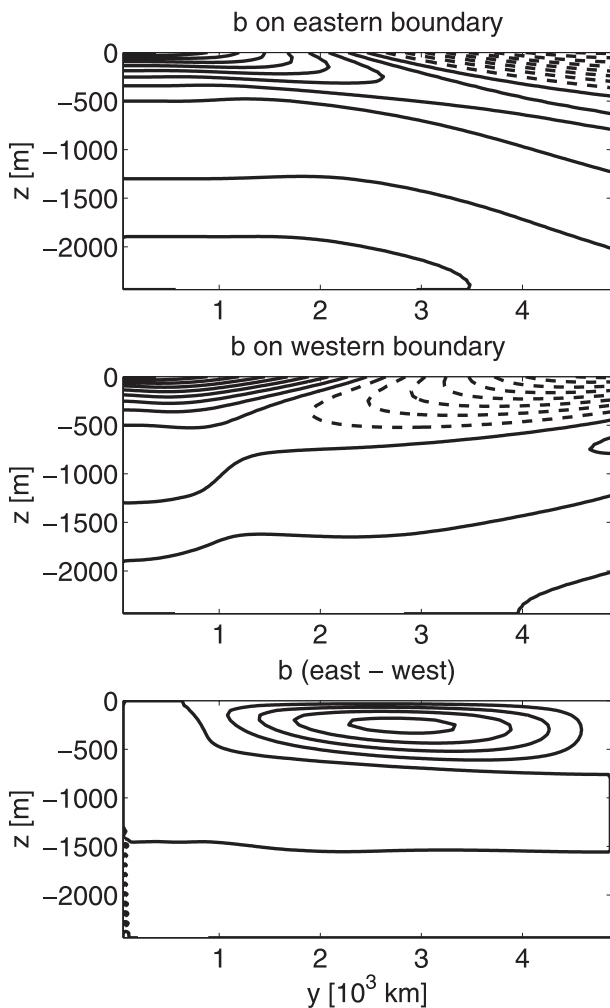


FIG. 9. (top) Buoyancy b on the eastern boundary, $x = x_e$, for the linear model; (middle) b on the western boundary, $x = 0$. (bottom) The difference between the fields in (top) and (middle), i.e., $b(x_e, y, z) - b(0, y, z)$. The fields should be compared to those for the eddy-resolving computation shown in Fig. 3. The CI is $2 \times 10^{-3} \text{ m s}^{-2}$. Negative values are dashed.

(Fig. 9) shows remarkable agreement. The largest discrepancy occurs in the east–west difference in the subtropical region: this is the wind-driven subtropical cell for which horizontal advection of buoyancy, neglected here, is essential (Luyten et al. 1983; Rhines and Young 1982).

The structure of the linear solution (43) together with the effective boundary condition (33) readily explains the downward and northward tilt of the isopycnals on the eastern boundary and the downward and southward tilt on the western boundary. We can approximately solve the buoyancy on the meridional boundaries by expanding the effective boundary conditions in vertical modes so that $\partial_z^2 \rightarrow -k_n^2$. Neglecting

the contribution from the distant boundary, we can make the approximation

$$\hat{b}_{\hat{z}\hat{z}\hat{x}} \sim \pm k_n^2 \lambda_{e,w} \hat{b}. \quad (54)$$

The plus sign in (54) applies to the east and the minus sign applies to the west. We can approximate $\lambda_{e,w}$ with the low-mode ($k_n \ll 1$) expansion of (45), that is,

$$\lambda_e \approx \frac{\hat{y}^2}{4} k_n^4, \quad \lambda_w \approx (k_n \hat{y})^{-2} + \frac{\hat{y}^2}{4} k_n^4. \quad (55)$$

Using these approximations in (54), and replacing $-\kappa_n^2 \rightarrow \partial_z^2$, the approximate effective BCs become

$$\frac{\hat{y}^3}{4} \hat{b}_{\hat{z}\hat{z}\hat{z}\hat{z}\hat{z}} = \hat{b}_{\hat{y}} \quad \text{at } x = X_e, \quad (56)$$

$$\frac{\hat{b}}{\hat{y}} - \frac{\hat{y}^3}{4} \hat{b}_{\hat{z}\hat{z}\hat{z}\hat{z}\hat{z}} = \hat{b}_{\hat{y}} \quad \text{at } x = 0. \quad (57)$$

Then (56) is a hyperdiffusion equation whose solution depends on the similarity variable $\eta_e = (\hat{z} - z_0)\hat{y}^{-2/3}$, and (57) is a hyperdiffusion equation whose solution is $\hat{b}(\hat{y}, \hat{z}) = \hat{y} \phi(\eta_w)$, with the similarity variable given by $\eta_w = (\hat{z} - z_0)(1 - \hat{y}^4)^{-1/6}$. Contours of these similarity variables are shown in Fig. 10 and they illustrate how the slope of the isopycnals on the eastern and western boundaries arises (cf. with Fig. 9). The imposed surface buoyancy distribution is carried at depth along the contours shown in Fig. 10.

The similarity solutions cannot hold along the whole meridional span of the boundaries because $b_e = b_w$ at $\hat{y} = 0, 1$. Given the sense of propagation of the similarity variables, b_w has to adapt to b_e at $\hat{y} = 1$, while b_e has to match b_w at $\hat{y} = 0$. Thus the buoyancies on the east and west boundaries, although they have a qualitatively different scaling [cf. (23) with (40)], are interdependent.

The linear solution in the interior, illustrated in Fig. 11 by three plan views at representative depths, shows the general southwest to northeast slant of the isopycnals, with a reversal of the north–south gradient at depth. The reversal is apparent in the buoyancy on the eastern boundary and the SW to NE slant can be inferred by conceptually connecting the isopycnals on the two boundaries in Fig. 9. In comparison with the eddy-resolving computation, shown in Fig. 12, the linear solution lacks the narrow scales of the western boundary current and its extension on the western side: the horizontal scale in the linear solution is δ_p defined in (23), and for values of κ appropriate for the western boundary (cf. Fig. 7) δ_p should be smaller than what is shown here. The horizontal advection of buoyancy by the barotropic flow near the western boundary is also

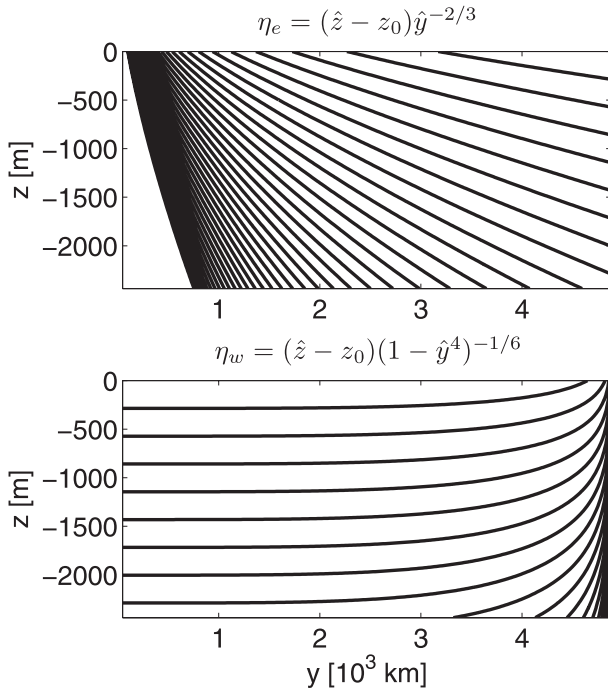


FIG. 10. (top) Contours of the similarity variable, η_e , of the hyperdiffusion equation associated with the effective boundary condition on the eastern boundary; compare with the top panel of Fig. 9. (bottom) The similarity variable η_w of the diffusion equation associated with the effective boundary condition on the western boundary; compare with the middle panel of Fig. 9. The similarity variables propagate the surface buoyancy signal downward along the eastern and western boundaries. The value chosen for z_0 is 3.

important in the eddy-resolving computation, but this process is neglected in the linear model. Otherwise, the linear solution captures the tilt of the isopycnals and the reversal of north–south gradients with depth with remarkable fidelity.

The linear solution shares qualitative features with the numerical solutions of the noninertial thermocline solutions of Colin de Verdière (1989), which include horizontal advection of buoyancy. As in that article, the solution is dominated by the buoyancy forcing rather than the wind forcing, as evidenced by the smallness of the parameter μ , defined in (25).

c. The strength of the MOC

The east–west buoyancy difference is an important quantity because it determines the MOC (Hirschi and Marotzke 2007; Marotzke 1997). On the basin scale, it is appropriate to neglect the viscous stress in (8) and use this approximate relation for v in (1). Integrating in the vertical and requiring that Ψ vanishes at $z = 0$ and $z = -H$ gives (2). Thus, given the wind stress and Δb ,

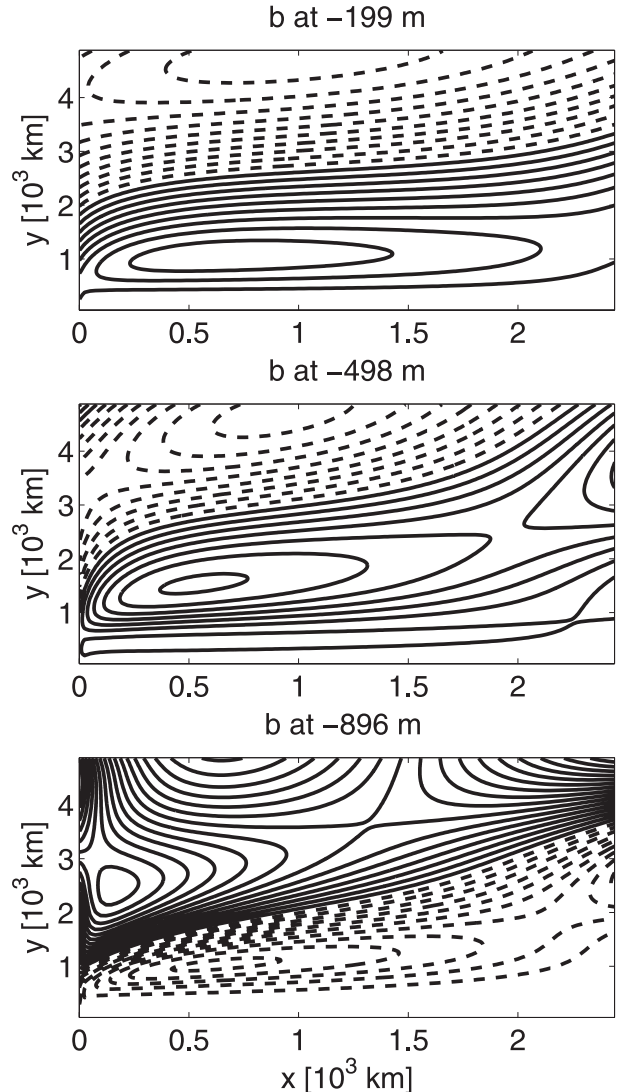


FIG. 11. Three plan views of the buoyancy for the linear solution (43) at various depths. The northeast to southwest tilt is dictated by the geometry of the buoyancy on the eastern boundary. (bottom) The reversal of the north–south buoyancy gradient at depth can be seen in the boundary values as well (cf. the top and middle panels in Fig. 9). The contour interval is (top) $1 \times 10^{-3} \text{ m s}^{-2}$, (middle) $0.4 \times 10^{-3} \text{ m s}^{-2}$, and (bottom) $1 \times 10^{-4} \text{ m s}^{-2}$. Negative values are dashed.

the time-averaged MOC can be estimated to a very good approximation. Using the diagnostic (2) for the linear model gives the MOC shown in Fig. 13, which compares well with the nonlinear computation shown in Fig. 1. Again, the linear model works best in the sub-polar region, and the inadequate description of the subtropical cell in the buoyancy difference is reflected in the estimate of Ψ . The linear planetary geostrophic model is also unable to reproduce the cross-equatorial abyssal cell seen in Fig. 11.

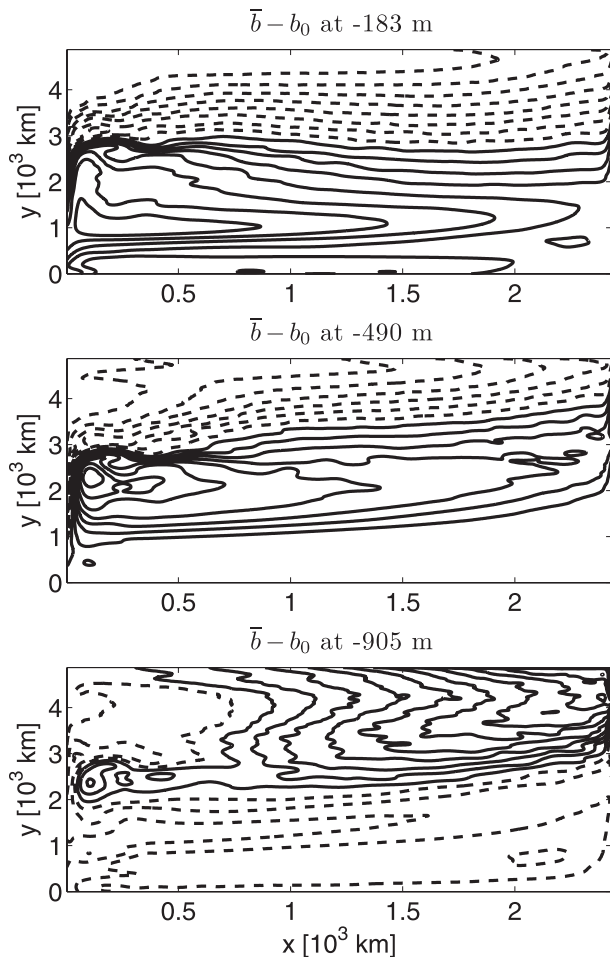


FIG. 12. Three plan views of the time-averaged buoyancy perturbations (i.e., the departures from the time and horizontal average) for the eddy-resolving computation at various depths. The main features of NE to SW tilt and N-S gradient reversal with depth are captured by the linear model (cf. Fig. 11). The CIs are (top) $1 \times 10^{-3} \text{ m s}^{-2}$, (middle) $0.4 \times 10^{-3} \text{ m s}^{-2}$, and (bottom) $1 \times 10^{-4} \text{ m s}^{-2}$. Negative values are dashed.

The diagnostic (2), together with the scaling discussed in section 3c, reveals the scaling of the MOC: because the depth of the thermocline on the western boundary, h_G , is larger than that on the eastern boundary, h , it dominates the integral in (2). We thus have

$$\Psi \sim (h_G^2 g' + H\tau_0)/(BL), \quad (58)$$

where h_G is the vertical scale in (40). Thus, without wind stress, the MOC scales like the square of the thermocline depth on the western boundary. According to (40) the MOC scales as $\Psi \sim g'[x_e \kappa_v / (\beta N^2)]^{1/2}$, a scaling that we have verified with the solution (43).

In nonlinear models of the oceanic circulation, N^2 is part of the solution and it is tempting to identify h_G

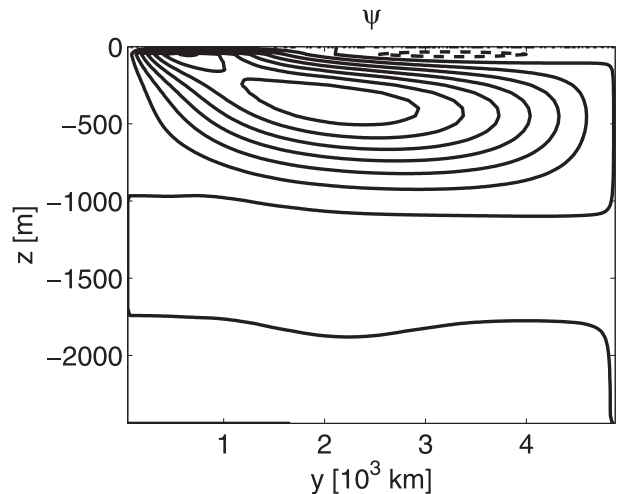


FIG. 13. The overturning streamfunction Ψ for the linear model accurately describes the eddy-resolving model MOC in the sub-polar region (top panel of Fig. 1), but only qualitatively in the subtropical region. The CI is 1 Sv.

as the scale height for the basic stratification (i.e., $N^2 \sim g'/h_G$). Using this hypothesis in (40), the scale of penetration of the surface buoyancy gradient in the interior is $h_G \sim (\beta L^2 \kappa_v x_e / g')^{1/3}$. Using this nonlinear scale we find that the MOC scales as

$$\Psi \sim (\kappa_v^2 x_e^2 L g' / \beta)^{1/3}. \quad (59)$$

This is the classical scaling of the buoyancy-driven MOC (Welander 1971; Vallis 2000). Notice that although the scaling is determined by the buoyancy value in a region where diapycnal diffusion is negligible and eddy diffusion is important, the final scaling depends on κ_v but not on κ .

Thus, the scaling for the MOC is determined by the depth of the thermocline on the western boundary. This is not to say that the buoyancy on the eastern boundary is irrelevant: for reasonable parameter values, h and h_G are comparable and Δb is very different from b_w (cf. Fig. 9). Specifically, we have that the ratio between the two scale heights is given by $h/h_G = (l/x_e)^{1/4}$, so that for narrow basins the influence of the eastern boundary is greater than for very wide basins.

A further question that can be explored with the linear solution is the relative importance of wind versus buoyancy forcing in determining the strength of the MOC. In the context of the linear model, this is done assuming that N^2 is fixed, although it is clear that this parameter would change in a full nonlinear calculation. In the expression (2) it is apparent that the explicit term due to the wind stress (i.e., the last integral on the

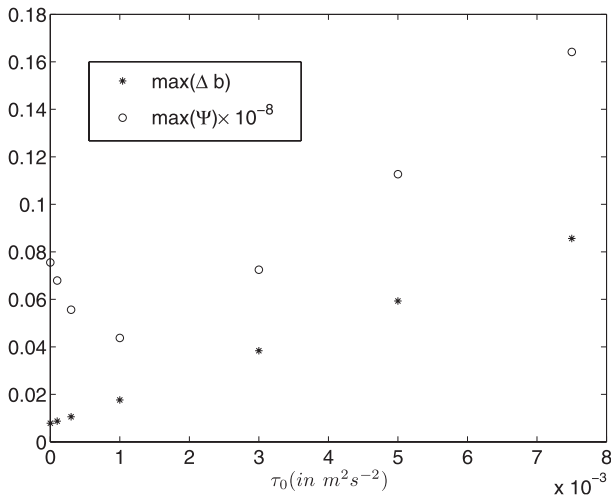


FIG. 14. The strength of the overturning streamfunction measured by the maximum of Ψ (below the Ekman layer) as a function of the strength of the wind stress, τ_0 (circles), and the maximum of the east–west buoyancy difference, Δb (asterisks), as a function of τ_0 for the linear model. The nonmonotonic behavior of Ψ for realistic values of τ_0 is due to the competing effects of the thermally indirect Ekman cell and the wind-driven contribution to the east–west buoyancy difference. The units of Ψ ($\text{m}^3 \text{s}^{-1}$) have been rescaled so that both quantities appear on the same plot. The units of b are m s^{-2} .

RHS) tends to decrease the strength of the MOC: this is the Ekman overturning cell, and it is thermally indirect in the region of the westerlies (i.e., opposite to the sense of circulation of the MOC). However, from (43), (44), and (49), Δb depends on the wind stress and the dependence is linear: this is illustrated in Fig. 14, which shows that Δb linearly increases with τ_0 . Because of the thermally indirect Ekman cell, the strength of the MOC decreases as τ_0 increases for small values of τ_0 , so that for realistic values of the wind stress, $\tau_0 = O(10^{-4} \text{ m}^2 \text{ s}^{-2})$, Ψ has a nonmonotonic behavior. For large values of the wind stress ($\tau_0 > 10^{-3} \text{ m}^2 \text{ s}^{-2}$), the increase due to Δb overcomes the decrease due to the reverse Ekman cell, and Ψ increases monotonically with τ_0 . However, this regime may be outside the range of validity of linear theory.

d. Boundary upwelling

The effective boundary conditions replace the detailed dynamics of the viscous boundary layer, and they allow the calculation of the vertical velocity *integrated across* the boundary layer. From (14), or equivalently (3), the integral of the vertical velocity across the viscous boundary layer on the eastern boundary, of width δ , is given by (a similar relation can be obtained on the western boundary)

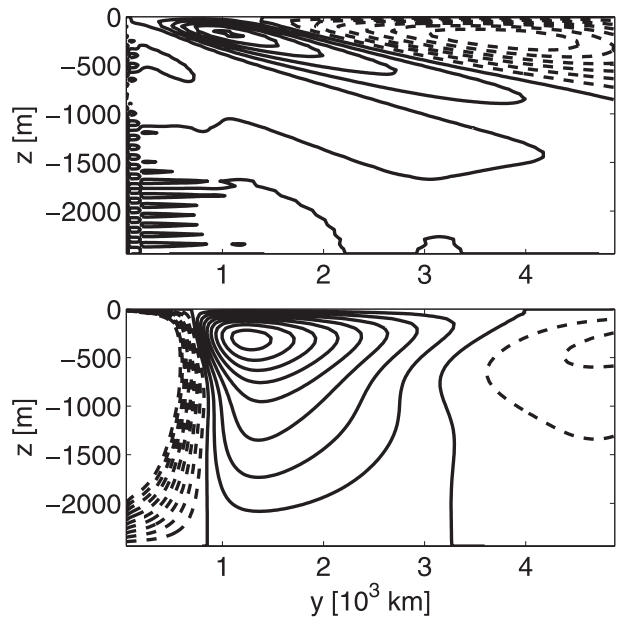


FIG. 15. The vertical velocity integrated across the (top) eastern and (bottom) western viscous boundary layers. The CI for the western boundary layer is $1 \text{ m}^2 \text{ s}^{-1}$, while on the eastern boundary layer it is $0.25 \text{ m}^2 \text{ s}^{-1}$. The solution shows strong downwelling near the equator on the west, but viscous effects cannot be neglected in this region, so the solution is not reliable there. On the east, there is buoyancy-driven downwelling in the thermocline in the subpolar region and most of the subtropics, while the tropics have wind-driven upwelling, which extends to the north below the thermocline.

$$\int_{x_e-\delta}^{x_e} w \, dx = -N^{-2} \kappa b_x \Big|_{x=x_e-\delta} + O(\delta). \quad (60)$$

The RHS can be calculated from the interior solution and it is shown in Fig. 15. The eastern boundary vertical velocity is dominated by buoyancy-driven downwelling near the surface, with wind-driven upwelling confined to the tropics. The downwelling in the upper portion of the boundary layer is necessary to return the surface eastward interior flow associated with the negative meridional temperature gradient (cf. top panel of Fig. 11). Conversely, the western boundary layer experiences upwelling. Given the basic stratification, N^2 , this results in higher buoyancy on the eastern boundary compared to the western boundary, so that Δb is positive as shown in Fig. 9 (bottom panel) (cf. Colin de Verdière 1988).

Below the main thermocline there is weak upwelling in the eastern boundary layer, associated with the interior westward flow due to the reversed meridional gradient (cf. bottom panel of Fig. 11). The vertical velocity in the eastern boundary layer compares very well with that found in the eddy-resolving model,

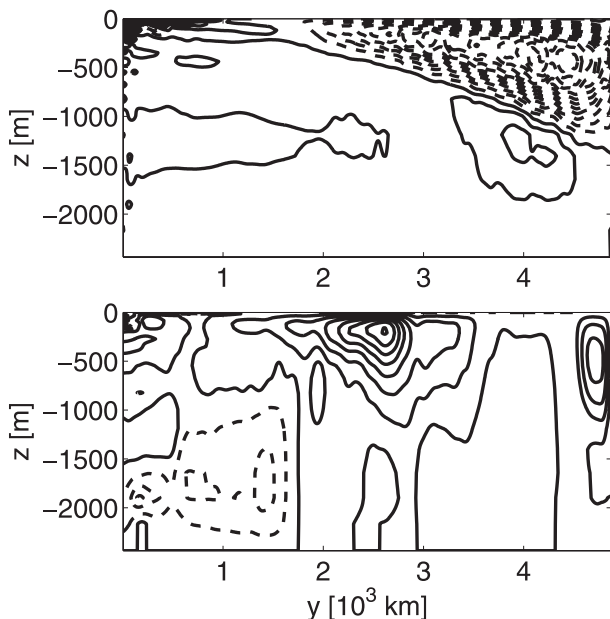


FIG. 16. The vertical velocity integrated across the (top) easternmost 54 km and (bottom) westernmost 54 km for the eddy-resolving model described in appendix A. The CI for the western boundary layer is $1 \text{ m}^2 \text{ s}^{-1}$, while on the eastern boundary layer it is $0.25 \text{ m}^2 \text{ s}^{-1}$. The fields have been smoothed in the y direction with a 30-point (163 km) Hanning window to remove the grid modes associated with hydrostatic convection.

shown in Fig. 16, and with previous analysis of the three-dimensional circulation (Colin de Verdière 1988, 1989).

The vertical velocities are much larger in the western boundary layer (cf. the contour interval for the two panels in Figs. 15, 16) and they reflect the compensation to the interior Ekman vertical velocity pattern (cf. the wind stress distribution shown in Fig. 8). In particular, there is strong downwelling near the equator that balances the strong interior Ekman suction at those latitudes. This downwelling cell is not present in the eddy-resolving simulation.

There are two reasons for the discrepancy on the western boundary. First, the solution (43) with (45) has a singularity in the x derivative at the single point $x = 0$, $y = 0$. Thus, even though the buoyancy is regular at the equator, the vertical velocity becomes infinite at $y = 0$. The singularity is due to a term behaving as $\hat{b} \sim \exp(-x/y^2)$ near the origin: this is the term multiplying c_n , and its form arises from the leading-order behavior near the equator $\lambda_w \lim_{y \rightarrow 0} (k_n y)^{-2}$. We believe that this weak singularity is cured by viscosity or diffusion in the y direction.

Second, as noted earlier, the effective BC (7) is not accurate at the western boundary where horizontal ad-

vection of buoyancy and momentum by the mean flow are large. Thus, the relationship (60) breaks down at the western boundary.

5. Discussion

Motivated by the results of an eddy-resolving computation, we have explored the effects of eddy buoyancy fluxes near the solid boundaries, with special emphasis on the eastern wall. We find that the requirement of a quasi-adiabatic flow leads to a mean ageostrophic circulation near the eastern (and western) boundary with strong upwelling (or downwelling) next to the solid walls, balanced by the eddy flux. The ageostrophic cell has a velocity component in the direction normal to the wall that cancels the baroclinic geostrophic velocity at the boundary, allowing a mean alongshore buoyancy gradient on both the eastern and western boundaries. The geostrophic constraint for the normal velocity is broken in a thin boundary layer where viscous (or Reynolds) stresses become important. For Newtonian friction, the thickness of the boundary layer is $Nhf^{-1}\sqrt{\nu/\kappa}$ (cf. Pedlosky and Spall 2005), where h is the dynamically determined depth near the boundary. The viscosity $\nu \approx 10 \text{ m}^2 \text{ s}^{-1}$ in the eddy-resolving model is much smaller than the eddy diffusivity, κ , associated with the resolved eddy buoyancy fluxes, and this viscous boundary layer is below the model's resolution. We find that it is not necessary to resolve the details of the viscous boundary layers if only the interior flow is of interest. Instead, *effective boundary conditions* for the interior flow can be applied. The effective boundary conditions relate the alongshore buoyancy gradient on the boundary to the eddy buoyancy flux at the outer edge of the boundary layer. The same eddy flux is also proportional to the vertical velocity integrated across the viscous/nonlinear boundary layer.

The consequences of the effective boundary conditions are explored in a model of the thermocline linearized around a prescribed mean stratification and a state of rest. This is G85's model with the addition of eddy fluxes of buoyancy parameterized as diffusion along isopycnals, with constant eddy diffusivity, κ .

The linearized model reveals that there are two vertical scales of the thermocline: one at the eastern boundary, h , and one at the western boundary, h_G . Only h_G has been considered in eddyless (i.e., $\kappa = 0$) models before; the thermocline depth at the eastern boundary, h , has been ignored in the past by considering the limit where the eddy diffusion vanishes. There are three east-west horizontal scales: l is the distance from the eastern boundary where eddy diffusion is important and the depth of the thermocline is h ; moving westward, on the basin

scale x_e , eddy diffusion is unimportant and the depth of the thermocline is h_G ; near the western boundary, eddy diffusion becomes important again on a scale δ_P . Both l and δ_P are scales of the order of 1000 km, intermediate between the basin scale and the viscous/nonlinear boundary layer.

The linear model is compared with an eddy-resolving computation in a parameter range outside the validity of the linear theory: horizontal and vertical variations of b are as large as the vertical variations due to the basic stratification, N^2 , around which the model is linearized. Remarkably, this leads to an accurate description of the buoyancy distribution on both the eastern and western boundaries, indicating that the effective boundary condition is a good approximation at the seaward edge of the thin viscous/inertial boundary layers. Of course, the specifications of the basic stratification and of the eddy fluxes of buoyancy are essential to determine the linear answer, while they are part of the solution in the nonlinear problem.

We find that even though the effective boundary condition is not accurate on the western boundary (due to the neglect of buoyancy advection), the buoyancy distribution is accurately described there. Presumably, meridional advection is so large on the western boundary that buoyancy is homogenized in the meridional direction and thus meridional transport is quenched. Indeed, the main difference between the western boundary buoyancy in the linear model and in the eddy-resolving model is that the latter has meridional gradients confined to the intergyre front. The neglect of horizontal advection by the mean flow near the western boundary can be relaxed: it is possible to generalize the effective boundary conditions (7) to include advection by a western-intensified barotropic velocity field. For consistency, the advection by the barotropic field must be included in the interior dynamics. This leads to a linear model as well, but one not amenable to simple analysis: it will be the subject of future study.

The linear model also gives a qualitatively correct description of the interior buoyancy distribution, especially in the subpolar gyre, where the ventilation dynamics are not important. However, the linear model has less east–west asymmetry than the nonlinear model: this is partly due to the choice of a constant κ , so that $l \sim \delta_P$, while δ_P should be substantially smaller than l if the eddy diffusivity is smaller at the western boundary; furthermore, the imprint of the wind-driven barotropic flow is absent in this linear formulation.

Because of the successful description of the east–west buoyancy difference, the linear model predicts well the strength of the MOC, whose maximum is at the subpolar/subtropical gyre boundary. The scaling of the

MOC strength is set by the depth of the thermocline at the western boundary h_G and is given by $\psi \sim g'(x_e \kappa_v / \beta N^2)^{1/2}$. Assuming that the stratification is internally determined (i.e., $N^2 \sim g'/h_G$), rather than prescribed as in the linear model, recovers the $\kappa_v^{2/3}$ law found in nonlinear models (Welander 1971; Vallis 2000).

Although the scaling of the MOC is determined by the depth of the thermocline on the western boundary, Δb is strongly influenced by b_e , not just b_w . This is because for typical oceanographic values $h_G \sim h$. The connection between the MOC and the boundary buoyancy suggests that processes local to the coasts are important for the global mass transport: presumably, local alongshore winds (excluded in the present treatment) also contribute to the buoyancy distribution on the eastern boundary and thus ultimately to the MOC.

Confining the eddy buoyancy fluxes near the eastern boundary would allow buoyancy gradients in the upper portion of the “shadow zone” to be matched to the ideal thermocline solutions in the interior (cf. Pedlosky 1983). Given the westward propagation sense of the potential vorticity conserving solution, it would be interesting to explore the influence of the effective BC on the interior PV distribution.

Acknowledgments. This research was supported by the Office of Science (BER) U.S. Department of Energy, Grant DE-FG02-01ER63252. We acknowledge the National Center for Computational Sciences at Oak Ridge National Laboratory, San Diego Super Computer Center, and NERSC for computational resources used in support of this project. We are grateful to Bill Young and Rick Salmon for several helpful conversations. Comments by two anonymous reviewers are gratefully acknowledged.

APPENDIX A

The Eddy-Resolving Run

We employ the Massachusetts Institute of Technology General Circulation Model [MITgcm; see Hill et al. (1999) and the references therein] to integrate the hydrostatic primitive equations in a simple flat-bottomed, equatorially centered, double-hemisphere, rectangular domain with a zonally periodic channel occupying the southernmost 1200 km of the domain and extending to the bottom. The approximate zonal and meridional extents of the domain are $x_e = 2400$ km and $L = 9800$ km, respectively, and the depth is $H = 2400$ m. This choice of domain size (narrow and shallow compared to a typical oceanic basin) is dictated by computational constraints.

Experiments with a non-eddy-resolving model, in which the effects of eddies are parameterized, have shown that increasing the domain size does not greatly alter the qualitative features of the circulation.

The momentum and thermodynamic equations are discretized on a fine Cartesian horizontal grid with grid spacing $\Delta x = \Delta y = 5.4$ km. The vertical grid has 20 levels with grid spacing that varies from 13 m at the surface to 275 m at the bottom. The levels are distributed such that vertical differences are second-order accurate. The use of a Cartesian grid—chosen for analytical simplicity—is somewhat nonstandard, but we have found that it does not alter the qualitative features of the circulation. Consistent with the choice of a Cartesian grid, the variation of the local planetary rotation rate is represented by a simple β plane, $f = \beta y$, with $\beta = 2.3 \times 10^{-11} \text{ m}^{-1} \text{ s}^{-1}$.

The momentum equations are forced by a specified surface wind stress, symmetric around the equator, whose Northern Hemisphere portion is shown in Fig. 8. Dissipation is provided by horizontal Laplacian viscosity with $\nu = 12 \text{ m}^2 \text{ s}^{-1}$, vertical viscosity with $\nu_V = 3 \times 10^{-4} \text{ m}^2 \text{ s}^{-1}$, and horizontal biharmonic friction with coefficient $\nu_4 = 9 \times 10^8 \text{ m}^4 \text{ s}^{-1}$. The horizontal Laplacian viscosity is chosen to have the minimum value necessary to resolve the Munk layer on the western boundary and the vertical Laplacian and horizontal biharmonic friction coefficients are chosen to have the minimum value necessary to ensure numerical stability. To relieve the model of having to resolve the turbulent bottom boundary layer, the bottom boundary condition is no-stress and a linear drag with coefficient $r = 1.1 \times 10^{-4} \text{ m s}^{-1}$ is applied as a body force in the bottom grid cell.

Density is a linear function of temperature only, so the thermodynamic equation reduces to a forced advection–diffusion equation for the buoyancy. Advective fluxes are calculated using a third-order direct space–time scheme with a Sweby flux limiter that avoids the generation of unphysical temperature extrema. Buoyancy is diffused via Laplacian diffusion with a constant, isotropic diffusivity $\kappa = 9.8 \times 10^{-5} \text{ m}^2 \text{ s}^{-1}$, which is close to the value of $\kappa = 10^{-4} \text{ m}^2 \text{ s}^{-1}$ required by the classical advective–diffusive theories of the thermocline (Munk 1966; Munk and Wunsch 1998). The use of an isotropic diffusivity eliminates the possibility of spurious diapycnal fluxes in the presence of large isopycnal slopes (i.e., the Veronis effect; Veronis 1975) without compromising model stability. The buoyancy equation is forced by relaxation to a specified zonally uniform surface distribution $g'B(y)$ in the top grid point with a relaxation time scale of 11 days. The surface buoyancy distribution is shown in Fig. 8. The maximum south–

north buoyancy difference is 0.0164 m s^{-2} . The amplitude of the wind stress divided by the mean density is $\tau_0 = 1 \times 10^{-4} \text{ m}^2 \text{ s}^{-2}$, corresponding to a momentum flux per unity density of 0.1 N m^{-2} .

The experiment reported here (Figs. 2, 3, etc.) was started from rest and integrated with a time step of 610 s for 438 yr. At this point near-statistical equilibrium had been achieved and 4-yr running averages of the dynamical variables showed little variation except for a slow buoyancy drift in the bottom 275 m, equivalent to less than 0.2 mK yr^{-1} .

APPENDIX B

Derivation of (13)

In this appendix, the vorticity Eq. (13) is derived.

Taking the difference of the y derivative of (8) and the x derivative of (9) we find the vorticity equation

$$\beta v - fw_z = -\tau_{zy} + \nu \nabla^2 (v_x - u_y). \quad (\text{B1})$$

Taking the sum of the x derivative of (8) and the y derivative of (9) we find the divergence equation

$$-\beta u + f(v_x - u_y) = \nabla^2 p + \nu \nabla^2 w_z. \quad (\text{B2})$$

We have used (11) to eliminate the horizontal divergence in favor of w_z . Eliminating the vorticity, $v_x - u_y$, between (B1) and (B2) we find

$$\beta v - fw_z = -\tau_{zy} + \nu \nabla^2 \left(\frac{\nabla^2 p + \beta u + \nu \nabla^2 w_z}{f} \right). \quad (\text{B3})$$

Using (8) and (9) repeatedly to eliminate βv and βu , we obtain

$$\begin{aligned} \beta \frac{p_x}{f} = fw_z - f \left(\frac{\tau_z}{f} \right)_y + f \nu \nabla \cdot \left[\frac{\nabla^2 (\nabla p)}{f} \right] \\ + \nu^2 \nabla^2 \left(\nabla^2 \frac{w_z}{f} \right) + \nu^2 \beta \left[\nabla^2 \left(\frac{\nabla^2 v}{f^2} \right) + \frac{\nabla^2 (\nabla^2 v)}{f} \right]. \end{aligned}$$

Dividing by f and taking the z derivative we have

$$\begin{aligned} \beta \frac{b_x}{f^2} = w_{zz} - \left(\frac{\tau_{zz}}{f} \right)_y + \nu \nabla \cdot \left[\frac{\nabla^2 (\nabla b)}{f} \right] + \frac{\nu^2}{f} \nabla^2 \left(\nabla^2 \frac{w_{zz}}{f} \right) \\ + \nu^2 \frac{\beta}{f} \left[\nabla^2 \left(\frac{\nabla^2 v_z}{f^2} \right) + \frac{\nabla^2 (\nabla^2 v_z)}{f} \right]. \end{aligned} \quad (\text{B4})$$

The buoyancy Eq. (14) can be used to eliminate w in favor of b , but the last two terms on the RHS of (B4)

cannot be written in terms of b . However, it is clear that all terms multiplied by powers of ν are only important in side boundary layers.

In (13) we keep only the term proportional to ν and neglect all terms proportional to ν^2 . This allows application of the nonnormal horizontal flow condition. The first term on the RHS, w_{zz} , allows application of the condition of no horizontal flux of buoyancy.

To apply the no-slip condition the terms proportional to ν^2 need to be considered: these are the last three terms on the RHS of (B4). Of the terms proportional to ν^2 , the first one is the largest one in boundary layers because it has the most horizontal derivatives:

$$\frac{\nu^2}{f} \nabla^2 \left(\nabla^2 \frac{w_{zz}}{f} \right) \approx \frac{\nu^2}{f} \nabla^2 \nabla^2 \left(\frac{\kappa \nabla^2 b}{f N^2} \right). \quad (B5)$$

The other terms proportional to ν^2 are [cf. (B8)]

$$\nu^2 \frac{\beta}{f} \nabla^2 \left(\frac{\nabla^2 v_z}{f^2} \right) \approx \nu^2 \frac{\beta}{f} \nabla^2 \left(\frac{\nabla^2 b_x}{f^3} \right). \quad (B6)$$

Therefore, for small viscosity and unless $\kappa \ll \nu$, it is possible to write a single approximate potential vorticity equation in terms of b , given by

$$\begin{aligned} \beta \frac{b_x}{f^2} = & w_{zz} - \left(\frac{\tau_{zz}}{f} \right)_y + \nu \mathbf{V} \cdot \left[\frac{1}{f} \nabla^2 \left(\frac{\mathbf{V} b}{f} \right) \right] \\ & + \frac{\nu^2}{f} \nabla^2 \left(\nabla^2 \frac{w_{zz}}{f} \right) + H.O.T., \end{aligned} \quad (B7)$$

together with (14).

To determine the BC appropriate for (B7), additional manipulations are needed. Let us consider no-flow ($u = 0$) and no-slip ($v = 0$) on the meridional boundaries ($x = 0, x_e$). Taking the x and z derivatives of (B2) and eliminating u_x in favor of $v_y + w_z$ gives

$$f \nabla^2 v_z = \nabla^2 b_x + \nu \nabla^2 w_{zzx} - f w_{zzy} + \beta v_{yz}. \quad (B8)$$

Using this result in the vertical derivative of (8) and applying the condition $u = v = 0$ gives

$$f b_y = \nu \left[\nabla^2 b_x + \nu \nabla^2 w_{zzx} - f w_{zzy} \right] \quad \text{at } x = 0, x_e, \quad (B9)$$

which is a condition on the fifth x derivative of b , to be applied to (B7). If only the no-flow condition is enforced, the second term on the RHS of (B9) can be dropped [the last term on the RHS of (B9) is subdominant in the boundary layer].

An additional BC is needed if no-slip is enforced. This can be obtained by eliminating u from (9) by using (8), that is,

$$-f v = -p_x + \tau_z - \nu \nabla^2 \frac{p_y}{f} + \nu^2 \nabla^2 \frac{\nabla^2 v}{f}. \quad (B10)$$

Approximating the Laplacian operator with ∂_x^2 , the term v_{xxxx} can be eliminated by using the x derivative of (B1), u_x can be eliminated using (11), v_x can be eliminated using (B2), and v_{xx} can be eliminated using (9). After taking the z derivative to eliminate pressure in favor of b the BC is

$$\begin{aligned} 0 = & b_x - \tau_{zz} + \nu \left(\frac{b_{xx}}{f} \right)_y + \nu^2 \left(\frac{w_{zzxx}}{f} \right)_y \\ & + \nu w_{zzx} + H.O.T. \quad \text{at } x = 0, x_e. \end{aligned} \quad (B11)$$

This BC is to be applied *in addition* to the no-flux condition $\kappa \nabla b \cdot \hat{\mathbf{n}} = 0$ ($b_x = 0$ on the meridional boundaries) so that it is a condition on the fourth derivative of b (in the boundary layer $w N^2 \approx \kappa b_{xxzz}$).

It should be stressed that the dominant balance in the boundary layers for the *barotropic* pressure is rather different: all the terms involving w_z in (B4), (B9), and (B11) vanish when the vertical integral is considered. Thus, the boundary layer widths for the barotropic flow are independent of the eddy diffusivity, while κ is essential for the baroclinic flow.

REFERENCES

- Barclon, V., and J. Pedlosky, 1967: A unified linear theory of homogeneous and stratified rotating fluids. *J. Fluid Mech.*, **29**, 609–621.
- Colin de Verdière, A., 1988: Buoyancy driven planetary flows. *J. Mar. Res.*, **46**, 215–265.
- , 1989: On the interaction of wind and buoyancy driven gyres. *J. Mar. Res.*, **47**, 595–633.
- Gent, P., and J. C. McWilliams, 1990: Isopycnal mixing in ocean circulation models. *J. Phys. Oceanogr.*, **20**, 150–155.
- Gill, A. E., 1985: An explicit solution of the linear thermocline equations. *Tellus*, **37A**, 276–285.
- Hill, C., A. Adcroft, D. Jamous, and J. Marshall, 1999: A strategy for terascale climate modeling. *Proc. Eighth ECMWF Workshop on the Use of Parallel Processors in Meteorology*, Reading, United Kingdom, ECMWF, 406–425.
- Hirschi, J., and J. Marotzke, 2007: Reconstructing the meridional overturning circulation from boundary density and the zonal wind stress. *J. Phys. Oceanogr.*, **37**, 743–763.
- LaCasce, J. H., 2004: Diffusivity and viscosity dependence in the linear thermocline. *J. Mar. Res.*, **62**, 743–769.
- Luyten, J., J. Pedlosky, and H. Stommel, 1983: The ventilated thermocline. *J. Phys. Oceanogr.*, **13**, 292–309.
- Marchesiello, P., J. C. McWilliams, and A. Skchepetkin, 2003: Equilibrium structure and dynamics of the California Current System. *J. Phys. Oceanogr.*, **33**, 753–783.
- Marotzke, J., 1997: Boundary mixing and the dynamics of the three-dimensional thermohaline circulation. *J. Phys. Oceanogr.*, **27**, 1713–1728.

- Munk, W., 1966: Abyssal recipes. *Deep-Sea Res. I*, **13**, 1259–1262.
- , and C. Wunsch, 1998: Abyssal recipes II: Energetics of tidal and wind mixing. *Deep-Sea Res. I*, **45**, 1977–2010.
- Pedlosky, J., 1969: Linear theory of the circulation of a stratified fluid. *J. Fluid Mech.*, **35**, 185–205.
- , 1983: Eastern boundary ventilation and the structure of the thermocline. *J. Phys. Oceanogr.*, **13**, 2038–2044.
- , 1987: *Geophysical Fluid Dynamics*. 2nd ed. Springer-Verlag, 710 pp.
- , and M. A. Spall, 2005: Boundary intensification of vertical velocity in a β -plane basin. *J. Phys. Oceanogr.*, **35**, 2487–2500.
- Rhines, P. B., and W. R. Young, 1982: A theory of the wind-driven circulation. I. Mid-ocean gyres. *J. Mar. Res.*, **40** (Suppl.), 559–596.
- Salmon, R., 1986: A simplified linear ocean circulation theory. *J. Mar. Res.*, **44**, 695–711.
- , 1990: The thermocline as an “internal boundary layer.” *J. Mar. Res.*, **48**, 437–469.
- Samelson, R. M., and G. K. Vallis, 1997: Large-scale circulation with small diapycnal diffusion: The two-thermocline limit. *J. Mar. Res.*, **55**, 223–275.
- Stammer, D., 1997: Global characteristics of ocean variability estimated from regional TOPEX/POSEIDON altimeter measurements. *J. Phys. Oceanogr.*, **27**, 1743–1769.
- Stommel, H., and J. Webster, 1962: Some properties of the thermocline equations in a subtropical gyre. *J. Mar. Res.*, **20**, 42–56.
- Vallis, G. K., 2000: Large-scale circulation and production of stratification: Effects of wind, geometry, and diffusion. *J. Phys. Oceanogr.*, **30**, 933–954.
- Veronis, G., 1975: The role of models in tracer studies. *Numerical Models of the Ocean Circulation*, National Academy of Sciences, 133–146.
- Welander, P., 1971: The thermocline problem. *Philos. Trans. Roy. Soc. London*, **A270**, 415–421.
- Wolfe, C. L., and P. Cessi, 2009: Overturning circulation in an eddy-resolving model: The effect of the pole-to-pole temperature gradient. *J. Phys. Oceanogr.*, **39**, 125–142.
- Young, W. R., and G. Ierley, 1986: Eastern boundary conditions and weak solutions of the ideal thermocline equations. *J. Phys. Oceanogr.*, **16**, 1884–1900.